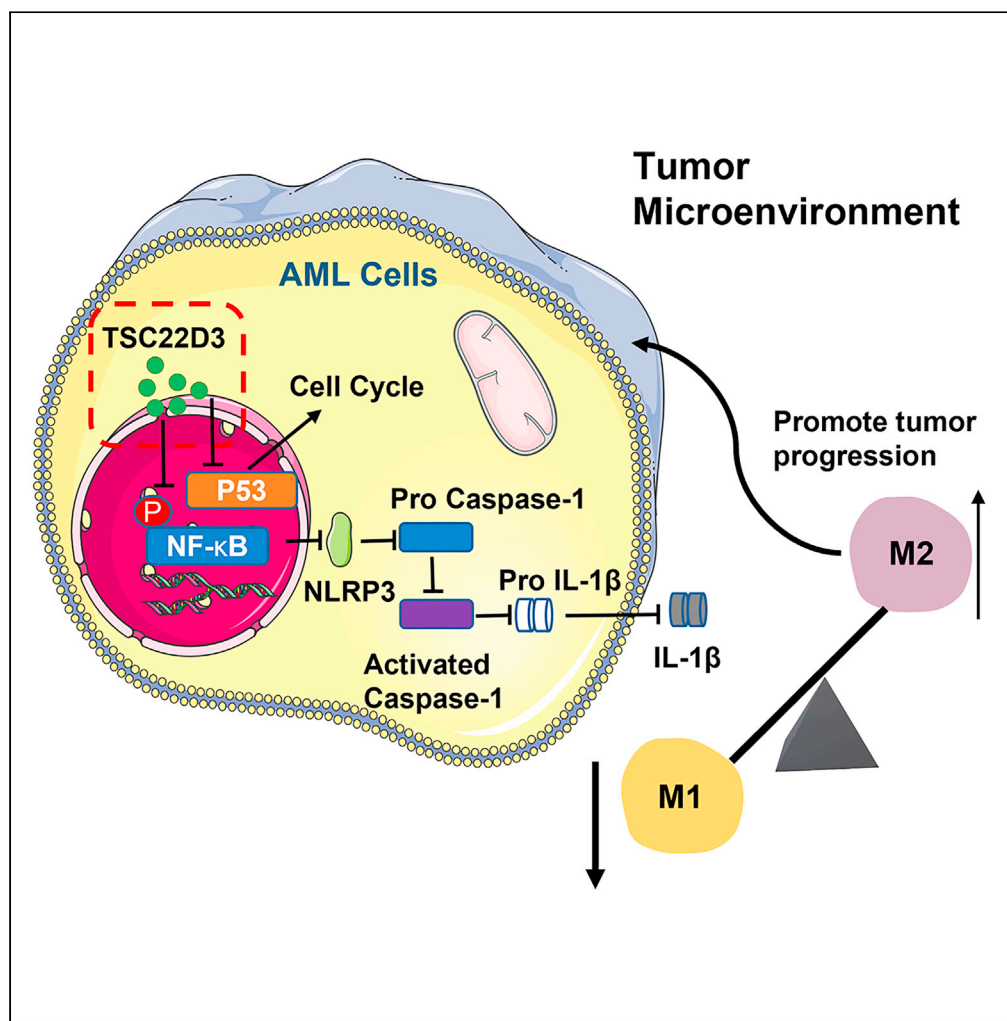**Article**

TSC22D3 as an immune-related prognostic biomarker for acute myeloid leukemia

Yang Li, Hanying Huang, Ziang Zhu, Shuzhao Chen, Yang Liang, Lingling Shu

liangyang@sysucc.org.cn (Y.L.)
shull@sysucc.org.cn (L.S.)

Highlights

TSC22D3 expression is closely associated with poor prognosis in AML

TSC22D3 regulates inflammatory immune response in AML tumor microenvironment

TSC22D3 inhibits the polarization of macrophage to M1-type

TSC22D3 attenuates inflammatory milieu through NF-κB/NLRP3 pathway

Article

TSC22D3 as an immune-related prognostic biomarker for acute myeloid leukemia

Yang Li,[1,2,4] Hanying Huang,[1,2,4] Ziang Zhu,[1,2,4] Shuzhao Chen,[1,2] Yang Liang,[1,2,*] and Lingling Shu[1,2,3,5,*]

SUMMARY

Acute myeloid leukemia (AML) is the type of hematologic neoplasm most common in adults. Glucocorticoid-induced gene *TSC22D3* regulates cell proliferation through its function as a transcription factor. However, there is no consensus on the prognostic and immunoregulatory significance of *TSC22D3* in AML. In the present study, we evaluated the correlation between *TSC22D3* expression, immunoinfiltration, and prognostic significance in AML. Knockdown of *TSC22D3* significantly attenuated the proliferation of Hel cells and increased sensitivity to cytarabine (Ara-c) drugs. Furthermore, *TSC22D3* reduced the release of interleukin-1β (IL-1β) by inhibiting the NF-κB/NLRP3 signaling pathway, thereby inhibiting macrophage polarization to M1 subtype, and attenuating the pro-inflammatory tumor microenvironment. In conclusion, this study identified *TSC22D3* as an immune-related prognostic biomarker for AML patients and suggested that therapeutic targeting of *TSC22D3* may be a potential treatment option for AML through tumor immune escape.

INTRODUCTION

Acute myeloid leukemia (AML) is a malignancy in which myeloid blasts proliferate in the hematopoietic system and is the most predominant leukemia in young adults aged 19–39 years.[1] Despite the use of advanced multimodal treatment strategies such as chemotherapy, radiotherapy, and allogeneic stem cell transplantation, AML remains one of the deadliest forms of leukemia.[2] AML is a genetically heterogeneous disease,[3] and chromosomal abnormalities play a crucial role in its diagnosis and treatment.[4] However, the underlying molecular mechanisms and pathogenesis of AML are still unclear, and only a few biomarkers are currently available for clinical treatment and prognosis. Although molecular-targeted therapy has made significant progress, many patients still experience relapse. Therefore, the development of prognostic biomarkers for AML diagnosis and treatment is crucial.

TSC22D3, which was first identified in 1997, encodes a glucocorticoid (GC)-induced anti-inflammatory leucine zipper (GILZ) protein.[5] The GILZ protein consists of 134 amino acids and is implicated in interference with various signal transduction pathways, including nuclear factor-κB (NF-κB),[6] activating protein-1 (AP-1),[7] Raf-MEK-ERK pathway,[8] and transcription factor forkhead box O3 (FoxO3).[9] Previous studies indicated that TSC22D3 was a GC-induced gene expression product that indirectly promotes glucocorticoid-mediated transcriptional inhibition.[10,11]

TSC22D3 was first linked to cancer in a study that identified that GILZ can disrupt the cell cycle and facilitate tumor progression by activating the AKT pathway in epithelial ovarian cancer (EOC) cells.[12] In chronic myeloid leukemia, GILZ promotes apoptosis in BCR::ABL1^{+} cells by inhibiting the mTORC2/AKT pathway.[13] PI3K/AKT inhibition can lead to apoptosis in multiple myeloma cells by increasing *TSC22D3* expression.[14]

Furthermore, a variant of the *TSC22D3* transcript called Long-GILZ (L-GILZ), which is upregulated by GCs, has similar functions to GILZ[15] and can activate the p53 pathway through interaction with p53 and murine double minute 2 (MDM2) to inhibit tumor growth.[16] Additionally, L-GILZ inhibits the growth of thyroid cancer cells and promotes carcinoma differentiation.[17] However, researchers have found that overexpressing *TSC22D3* can eliminate the tumor growth inhibitory effects of chemotherapy, while knockout of *TSC22D3* significantly attenuated the stress-induced immunosuppression in cancer and suggests that *TSC22D3* is a poor prognostic gene.[18] It is evident from these findings that *TSC22D3* plays key roles in both tumor

[1]State Key Laboratory of Oncology in South China, Collaborative Innovation Center for Cancer Medicine, Sun Yat-sen University Cancer Center, Guangzhou 510060, P.R. China

[2]Department of Hematological Oncology, Sun Yat-sen University Cancer Center, Guangzhou 510060, P.R. China

[3]State Key Laboratory of Pharmaceutical Biotechnology, The University of Hong Kong, Hong Kong 999077, P.R. China

[4]These authors contributed equally

[5]Lead contact

*Correspondence:
liangyang@sysucc.org.cn (Y.L.),
shull@sysucc.org.cn (L.S.)
https://doi.org/10.1016/j.isci.2023.107451

progression and immunity. Recently, a bioinformatic study has shown the expression and prognostic significance of TSC22D domain family genes in adult AML;[19] nevertheless, the potential role and prognostic significance of *TSC22D3* in AML are still unclear and need to be further clarified.

In the present study, we investigated the prognostic value of *TSC22D3* in AML and its effect on the immune infiltration of AML tumor microenvironment. Our results identified *TSC22D3* as an immune-related prognostic biomarker for AML patients. Mechanically, *TSC22D3* alleviated the pro-inflammatory tumor microenvironment by attenuating the polarization of macrophage to M1 subtype by inhibiting NF-κB/NLRP3 signaling pathway in tumor cells, suggesting that therapeutic targeting of *TSC22D3* may be a potential treatment strategy for AML.

RESULTS

Expression of *TSC22D3* is elevated in AML

To investigate the expression of *TSC22D3* in tumors, we first performed a combined analysis of The Cancer Genome Atlas (TCGA) and Genotype-Tissue Expression (GTEx) database to analyze the differences between normal and tumor samples. Our analysis indicated that *TSC22D3* was significantly highly expressed in several cancers, including glioblastoma multiforme (GBM), kidney renal clear cell carcinoma (KIRC), AML, brain low-grade glioma (LGG), and pancreatic adenocarcinoma (PAAD) (Figure 1A). To better understand *TSC22D3* expression during AML progression, we analyzed bone marrow samples from 62 non-leukemia (control), 164 myelodysplastic syndromes (MDS), and 202 AML patients in the GSE15061 dataset. Our study revealed that the expression of *TSC22D3* was significantly higher in patients with AML compared to both control subjects and patients with MDS (Figure 1B). Similarly, we observed a high expression of *TSC22D3* in AML compared to MDS in the GSE13159 dataset, which contained 74 controls, 206 MDS patients, and 542 AML patients (Figure 1C). To investigate the role of *TSC22D3* in AML, we divided AML patients into two groups based on the median expression of *TSC22D3* in the TCGA database and performed differential expression analysis. We obtained 1,154 differentially expressed genes (DEGs) of which 657 were upregulated and 497 were downregulated. Our analysis of the top 10 differential genes revealed that *TSC22D3* was co-expressed with several immune-related genes, including *IL1R2*, *SLC10A2*, *AREG*, interleukin (*IL*)-10, and *SDC2* (Figure 1D). Our findings indicated that *TSC22D3* expression is notably high in AML, which implies a potential connection between *TSC22D3* and immune response.

High expression of *TSC22D3* is associated with immunoinfiltration in the AML tumor microenvironment

After analyzing the differences, we formed a hypothesis that *TSC22D3* in AML is involved in the immune response. To delve deeper into this theory, we conducted Gene Ontology (GO) analysis of DEGs. The findings suggested that *TSC22D3*-related genes significantly impact multiple biological functions. These functions encompass the regulation of inflammatory responses, leukocyte proliferation, tumor necrosis factors production, cytokine production related to immune response, myeloid leukocyte differentiation, and macrophage migration (Figure 2A). To further investigate the relationship between *TSC22D3* expression and immune cells, we performed immunoinfiltration analysis. *TSC22D3* expression was positively correlated with macrophages, T helper-1 (Th1) cells, and Th17 cells and negatively correlated with T helper cells and mast cells (Figure 2B). As the expression of *TSC22D3* increased, the infiltration of macrophages (Figure 2C), Th1 cells (Figure 2D), and Th17 cells (Figure 2E) in the tumor microenvironment increased. We further investigated the association between *TSC22D3* expression and T cell immune checkpoints such as *PD-1*, *PD-L1*, and *CTLA-4*. *TSC22D3* expression was significantly corroborated with *PD-1* (Figure 2F) and *CTLA-4* (Figure 2H) expression in AML, but not with *PD-L1* (Figure 2G). Additionally, to explore the functional relevance of *TSC22D3*-associated genes, we conducted gene set enrichment analysis (GSEA) on DEGs using the curated gene set (c2.cp.v7.2.symbols.gmt) from the Molecular Signature Database (MSigDB) (https://www.gsea-msigdb.org/gsea/msigdb/index.jsp). The set of genes enriched in the *TSC22D3* high-expression group included IL-18, p53, IL-4 and IL-13, IL-1 family, and NF-κB signaling pathways (Figure 2I). These results demonstrated that *TSC22D3* influences the infiltration of immune cells and inflammation-related signaling pathways in the AML tumor microenvironment.

High expression of *TSC22D3* is closely related to poor prognosis in AML patients

We conducted an analysis of 148 AML patients with different cytogenetic risk profiles from the TCGA database, including 30 patients with favorable cytogenetic risk, 82 with intermediate cytogenetic risk, and 36
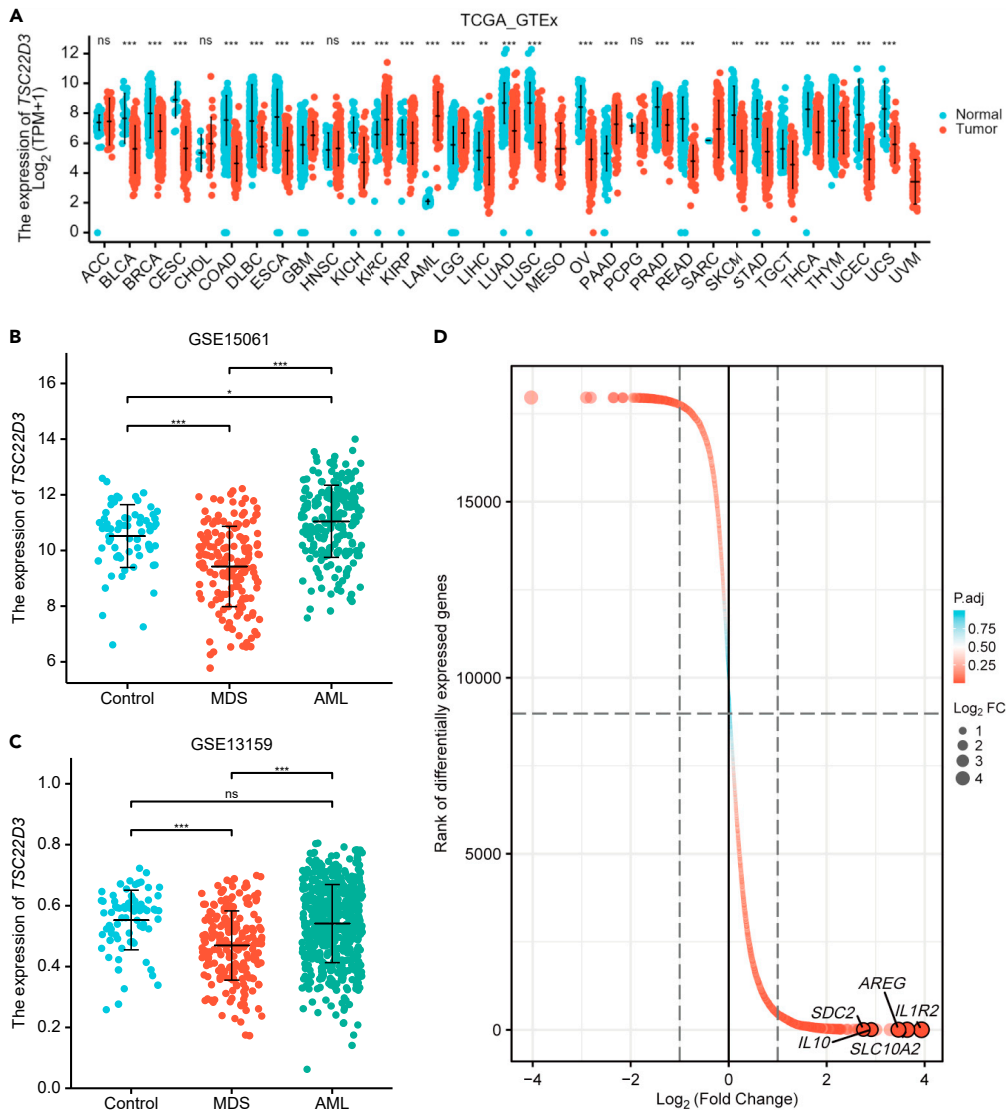
Figure 1. *TSC22D3* is highly expressed in AML

(A) TCGA and GTEx databases combined with pan-cancer analysis showed that *TSC22D3* was highly expressed in GBM, KIRC, AML, LGG, and PAAD. The full names corresponding to TCGA disease abbreviations are shown in Table S3.

(B and C) Using GSE15061 and GSE13159 datasets in the GEO database to further verify that *TSC22D3* was highly expressed in AML.

(D) *TSC22D3* was co-expressed with the immune-related genes *IL1R*, *SLC10A2*, *AREG*, *IL10*, and *SDC2*; |log2(FC)| > 1, p.adj <0.05. Data were expressed as mean ± SD (A-C). Abbreviations: p.adj, adjusted p value. Wilcoxon rank-sum test (A) was used to analyze two groups, and Kruskal-Wallis's test (B and C) was used to analyze multiple groups. Significant markers: ns, p ≥ 0.05; *, p < 0.05; **, p < 0.01; ***, p < 0.001.

with poor cytogenetic risk patients, to investigate the significance of *TSC22D3* expression on prognosis. The findings indicated that the *TSC22D3* expression increased progressively with increasing cytogenetic risk class (Figure 3A). The Kaplan-Meier (K-M) curve was utilized to evaluate the survival time of AML patients in groups with high *TSC22D3* versus low *TSC22D3*. We observed that TSC22D3^{-low} patients had significantly better 8-year overall survival (OS) rate than TSC22D3^{-high} patients (Figure 3B). Subgroup survival analysis indicated a positive correlation between *TSC22D3* expression and poor prognosis in patients who lacked mutations in *FLT3*, *IDH1 R132*, *IDH1 R140*, *IDH1 R172*, *RAS*, and *NPM1* (Figures 3C–3H). However, *TSC22D3* expression was not associated with poor prognosis in the *FLT3*, *IDH1 R132*, *IDH1 R140*, *RAS*, and *NPM1* mutation-positive subgroups (Figure S1). Furthermore, multivariate Cox regression analysis
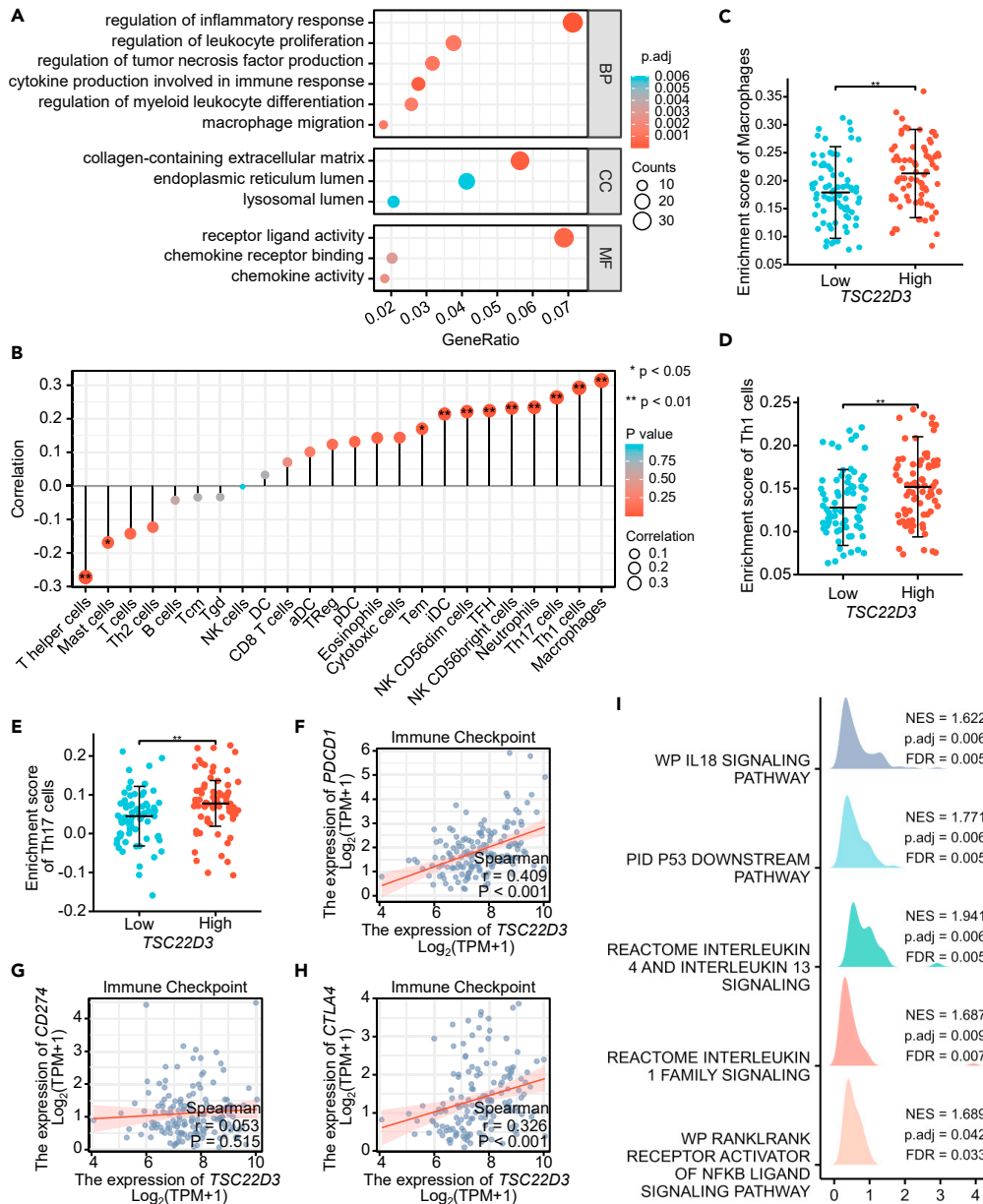
Figure 2. *TSC22D3* is highly associated with the AML immune microenvironment

(A) GO analysis showed that *TSC22D3*-related genes were mainly involved in the biological processes of inflammation and immunity.

(B) Correlation analysis between *TSC22D3* and enrichment scores of 24 immune cells by Spearman correlation analysis. The size of the circle represents the degree of correlation. The greater the height of the bar (distance from 0), the higher the degree of correlation. The depth of the circle represents the p value obtained by the correlation statistical method.

(C–E) The relationship between *TSC22D3* and the infiltrated macrophages (C), Th1 (D), and Th17 (E) lymphocytes.

(F–H) Scatterplots of the correlations between *TSC22D3* expression and *PD-1* (F), *PD-L1* (G), and *CTLA-4* (H) in AML.

(I) GSEA pathway enrichment analysis showed that TSC22D3-related differential genes could cause significant changes in different signaling pathways such as inflammation. Data were expressed as mean ± SD (C–E). Abbreviations: BP, biological process; CC, cell component; MF, molecular function; NES, normalized enrichment score; FDR, false discovery rate; r, correlation coefficient. Student's t test (C–E) was used for the analysis between the two groups. Significant markers: *, $p < 0.05$; **, $p < 0.01$.
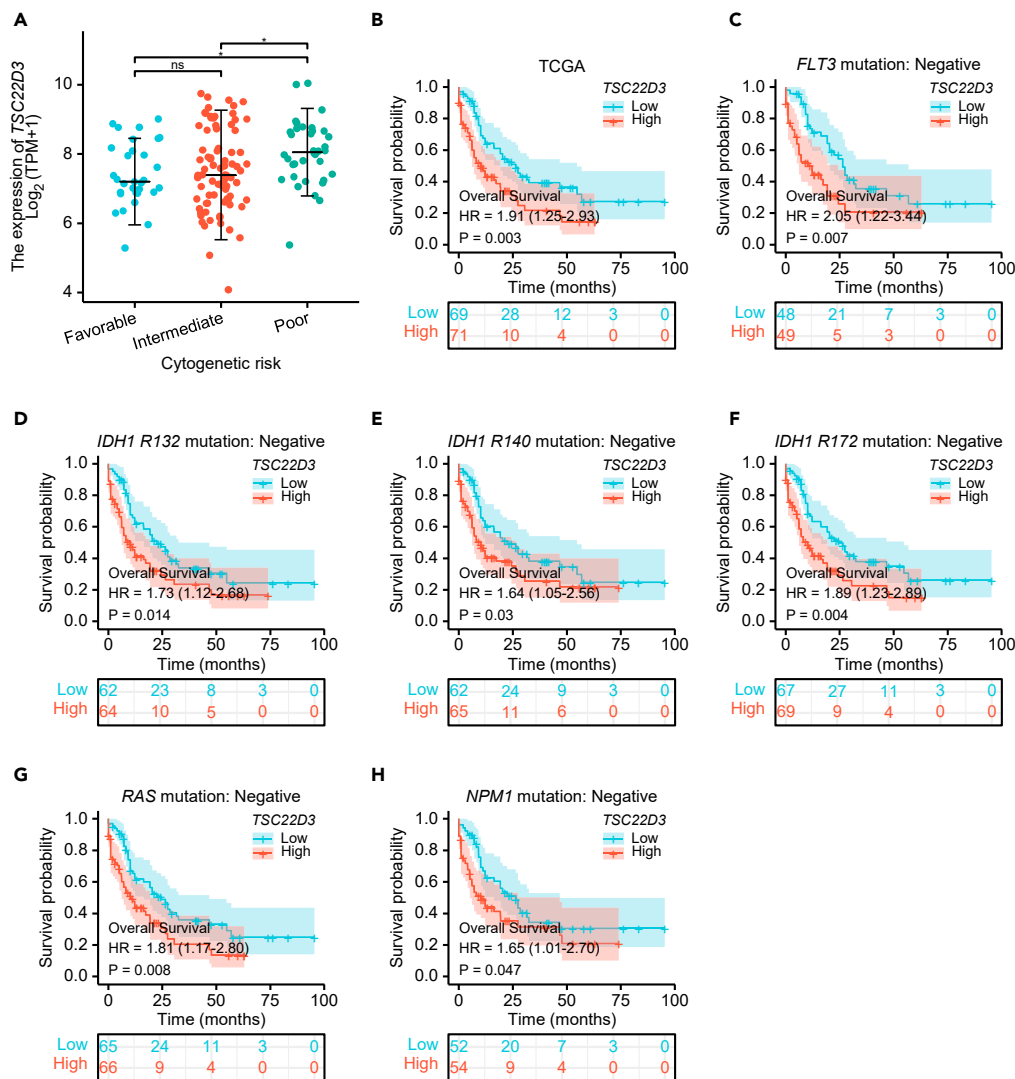
Figure 3. High expression of *TSC22D3* is associated with poor prognosis of AML

(A) The clinical correlation between *TSC22D3* expression and cytogenetic risk stratification of AML.

(B) OS curves between *TSC22D3*-high and *TSC22D3*-low patients with AML.

(C–H) High *TSC22D3* expression was associated with poor prognosis in the subgroups of mutation-negative genes including *FLT3* (C), *IDH1 R132* (D), *IDH1 R140* (E), *IDH1 R172* (F), *RAS* (G), and *NPM1* (H). The gene mutation-positive groups can be found in Figure S1. Cox regression analysis and prognostic modeling can be seen in Figure S2 and Table S4. HR > 1 indicates that the variable was a risk factor, and HR < 1 was a protective factor. Data were expressed as mean ± SD (A). Abbreviations: HR, hazard ratio. One-way ANOVA test (A) was used to analyze multiple groups of overall comparisons. Cox regression (C–H) was used for survival analysis. Significant markers: ns, p ≥ 0.05; *, p < 0.05.

revealed that age over 60 years, intermediate and poor cytogenetic risk, and high expression of *TSC22D3* were independent prognostic predictors (Table S4). To investigate the predictive effect of *TSC22D3* on AML prognosis, we constructed a prognostic prediction model utilizing the findings of a multivariate Cox regression analysis. The nomogram model used a ruler score to evaluate the conditions of each variable and calculate a total score to estimate the probability of the event taking place. The points assigned to each variable were adjusted on a scale of 1–100. A vertical line was drawn from the total point axis to the outcome axis to determine the probability of survival for AML patients at 1, 3, and 5 years. The model demonstrated good prediction efficiency, as evidenced by the consistency index (C-index) of 0.735 (Figure S2A). Additionally, we utilized the receiver operating characteristic curve (ROC) model to assess the prognostic predictive efficacy of *TSC22D3* expression. Area under curve (AUC) values for 1, 3, and 5 years
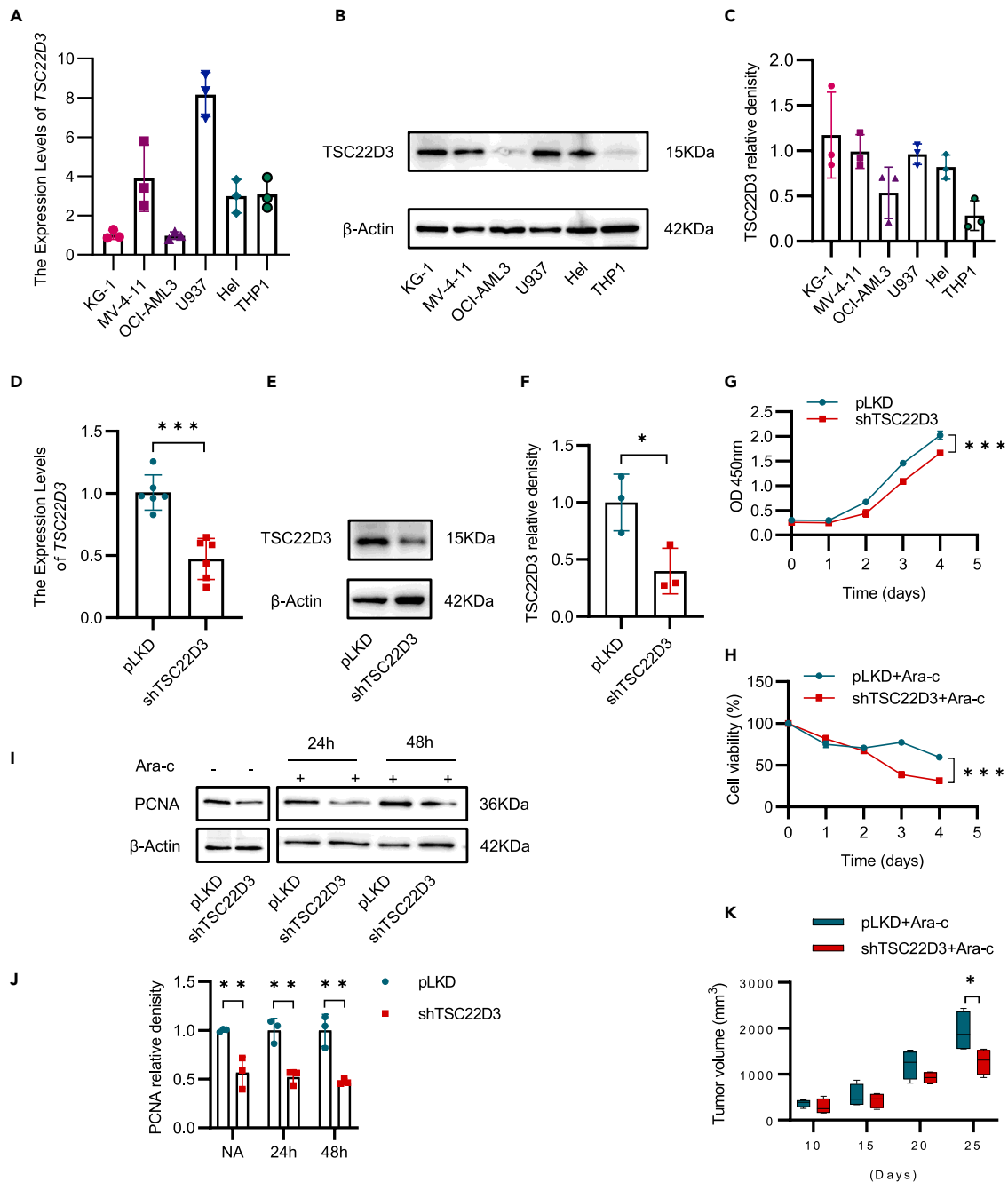
Figure 4. High expression of *TSC22D3* promotes the proliferation of AML cells and inhibits sensitivity to Ara-c

(A) The mRNA expression levels of *TSC22D3* in different hematologic tumor cell lines (n = 3).

(B) Western blot analysis of *TSC22D3* in different hematologic tumor cell lines.

(C) The normalized quantification of *TSC22D3* band density compared to β-Actin (n = 3).

(D) RT-qPCR analysis knockdown efficacy of Hel cells after transduction of pLKD vector or shTSC22D3 vector (n = 6).

(E) Western blot analysis knockdown efficacy of Hel cells after transduction.

(F) The normalized quantification of *TSC22D3* band density compared to β-Actin (n = 3).

(G) CCK-8 analysis for cell viability of Hel cells after transfected with shTSC22D3 vector or pLKD vector (n = 4).

(H) CCK-8 analysis for cell viability of Hel cells after transduction followed by 100 nM Ara-c treatment for 4 days (n = 4). EC50 values see Figure S3.

(I) Western Blot analysis of proliferation cell nuclear antigen (PCNA) in Hel cells transfected with shTSC22D3 vector or pLKD vector in the presence or absence of 100 nM Ara-c treatment for 24 h and 48 h.

(J) The normalized quantification of PCNA band density compared to β-Actin (n = 3).

Figure 4. Continued

(K) Analysis of proliferation of Hel cells after transfection in 4-6-week-old male BALB/c nude CDX treated with 20 mg/kg Ara-c every 3 days for 25 days (n = 4). Data were expressed as mean ± SD (A, C, D, F, G, H, and J) or min to max (K). Student's t test (D, F, and J) for two groups comparison and two-way repeated measures ANOVA (G, H, and K) analysis for multi-factor comparisons. Significant markers: *, p < 0.05; **, p < 0.01; ***, p < 0.001.

were 0.615, 0.587, and 0.618, respectively. These results suggested that the predictive power of *TSC22D3* expression is limited as the AUC values indicate low prediction efficiency (Figure S2B). To assess the model's performance, we generated a calibration plot that compares the predicted probabilities of survival with the actual outcomes. The calibration plot showed a bias-corrected line that closely resembled the ideal curve, which is the 45-degree line. This indicates that there is good agreement between the predictions and observations. The figure displays three lines that represent the comparison between the model's predicted survival probabilities for 1-year (blue), 3-year (red), and 5-year (green) periods, respectively, with the actual outcomes (Figure S2C). In conclusion, our findings indicated that increased *TSC22D3* expression is linked to a negative outcome for AML and may serve as a potential prognostic marker.

TSC22D3 promotes the proliferation of AML cells and reduces Ara-c sensitivity

To investigate the expression of *TSC22D3* in hematological tumor cell lines, we utilized real time quantitative polymerase chain reaction (RT-qPCR) and western blotting techniques to detect mRNA and protein expression. Our findings revealed relatively high levels of *TSC22D3* mRNA expression in U937, MV-4-11, Hel, and THP1 cell lines (Figure 4A), and *TSC22D3* protein expression was relatively high in KG-1, MV-4-11, U937, and Hel cell lines (Figures 4B and 4C). To study the impact of *TSC22D3* on tumor cells, Hel cells were transfected with the shTSC22D3 vector and pLKD vector, and the knockdown efficacy of *TSC22D3* was verified first. Our results indicated that both the mRNA levels (Figure 4D) and protein expression (Figures 4E and 4F) of *TSC22D3* were significantly reduced in the knockdown group compared to the control group. We investigated the regulatory role of *TSC22D3* by conducting the cell counting kit-8 (CCK-8) assay to determine cell proliferation and drug sensitivity *in vitro*. Knockdown of *TSC22D3* inhibited the growth rate of tumor cells (Figure 4G). Ara-c is a commonly used chemotherapy drug for treating AML. In our study, we found that the cell concentration for 50% of the maximal effect (EC50) of Ara-c on Hel cells was 155.6 nM (Figure S3A). Consistently, *TSC22D3* deficiency increased the sensitivity to Ara-c of Hel cells (Figure 4H). To further demonstrate the effect of *TSC22D3* on cell proliferation, we examined the expression of proliferation cell nuclear antigen (PCNA) protein, a marker of cell proliferation, in the presence and absence of 100 nM Ara-c treatment for 24 and 48 h. Knockdown of *TSC22D3* inhibited the expression of PCNA (Figures 4I and 4J). *In vivo*, the mouse cell-derived xenograft (CDX) model further confirmed that *TSC22D3*-deficient AML cells obviously alleviated the proliferation rate and tumor invasion (Figure 4K). The above results indicated that the knockdown of *TSC22D3* inhibits the growth of tumor cells and increases the drug sensitivity to Ara-c.

TSC22D3 inhibits apoptosis of tumor cells and affects cell cycle

As apoptosis is a crucial factor in the development and advancement of tumors, we sought to investigate whether *TSC22D3* regulates the apoptosis of AML cells. To this end, we measured the apoptosis rate of cells that were treated with 100 nM Ara-c or vehicle for 2 days. Interestingly, knockdown of *TSC22D3* did not cause apoptosis of tumor cells, but with the treatment of Ara-c, knockdown of *TSC22D3* could promote the apoptotic rate of tumor cells (Figures 5A and 5B). We consider that Ara-c exerts its antitumor effects mainly by inhibiting DNA polymerase, interfering with DNA replication, and affecting the cell cycle. We speculate whether *TSC22D3* affects cell proliferation, apoptosis, and sensitivity to Ara-c by influencing the cell cycle. To test this hypothesis, we used propidium iodide (PI) staining and flow cytometry to detect the cell cycle. We found that the knockdown of *TSC22D3* increased the Gap0 (G0) and Gap1 (G1) phases meanwhile inhibiting the synthesis (S) phase (Figures 5C and 5D). Consistently, after co-stimulated with Ara-c, knockdown of *TSC22D3* significantly increased the S stage but inhibited the Gap2 (G2) and mitosis (M) stage of AML cells (Figures 5E and 5F). The role of the p53 signaling pathway in regulating the cell cycle is widely recognized. To investigate the possible mechanism by which *TSC22D3* impacts the cell cycle, we conducted protein blotting to detect the expression of the p53 protein. Our findings, as revealed by western blot analysis, indicated that *TSC22D3* deficiency in AML cells leads to increased expression of p53 (Figures 5G and 5H), suggesting that *TSC22D3* may regulate the tumor cell cycle via interaction with p53.
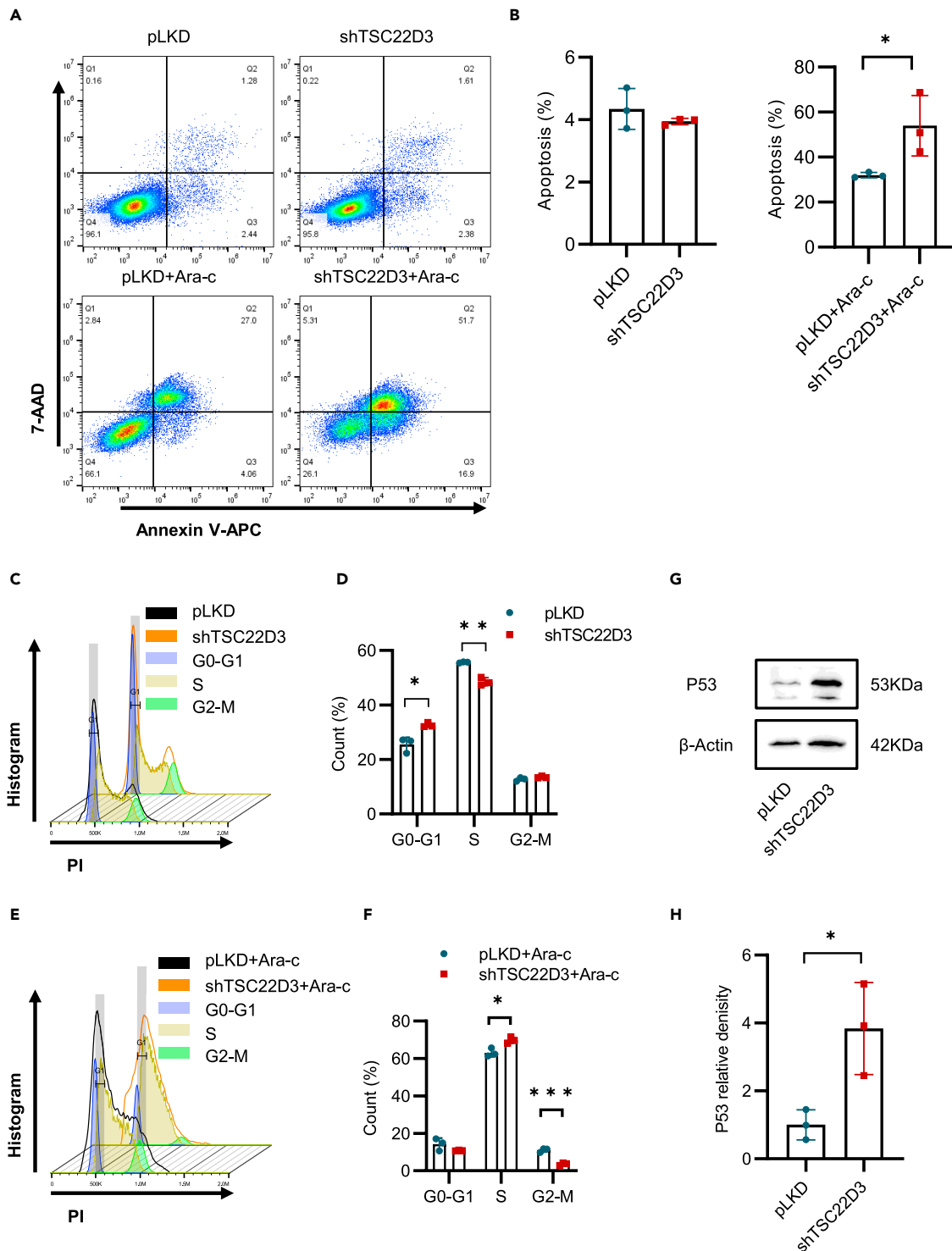
Figure 5. *TSC22D3* affects apoptosis and the cell cycle

(A) Representative fluorescence-activated cell sorting plots showed the frequencies of apoptotic Hel cells after transfected with shTSC22D3 vector or pLKD vector for 48 h in the presence or absence of 100 nM Ara-c treatment.

(B) Quantitative statistical analysis of Hel cells apoptosis percentage (n = 3).

(C) The staggered offset histogram analysis showed the percentage of different cell cycles of Hel cells after being transfected with the shTSC22D3 vector or pLKD vector.

(D) Quantitative statistical analysis of Hel cell cycle percentage (n = 3).

Figure 5. Continued

(E) The staggered offset histogram analysis showed the percentage of different cell cycles of Hel cells after transfected with shTSC22D3 vector or pLKD vector treated with Ara-c (100 nM) for 48 h.

(F) Quantitative statistical analysis of Hel cells cycle percentage treated with Ara-c (100 nM) (n = 3).

(G) Western blot analysis of protein expression levels of p53 in Hel cells after transfection.

(H) The normalized quantification of p53 band density compared to β-Actin (n = 3). Cell cycle model constraints were G2 peak = 2G1, G1 CV = G2 CV = 8.00. Data were expressed as mean ± SD (B, D, F, and H). Abbreviations: CV, coefficient of variation. Student's t test (B, D, F, and H) for two groups comparison. Significant markers: *, $p < 0.05$; **, $p < 0.01$; ***, $p < 0.001$.

TSC22D3 inhibits the infiltration and polarization of M1-type macrophages

To explore the specific role of *TSC22D3*-knocked tumor cells on the immune response, we used the co-culture of tumor cells and M0-type macrophages. Firstly, the induction of differentiation of THP1 cells into M1- and M2-type macrophages was verified (Figures S3B and S3C). The downregulation of *TSC22D3* resulted in increased levels of *CD80* and tumor necrosis factor-α (*TNF-α*) mRNA expression in M1 macrophages, while simultaneously decreasing the expression of *CD206* and *PPARγ* mRNA in M2 macrophages (Figures 6A and 6B). To assess the impact of *TSC22D3* knockdown in tumor cells on immunoinfiltration, we generated single-cell suspensions from CDX mouse model tumor tissues for flow cytometry analysis. The results showed that *TSC22D3*-knockdown tumor cells promoted infiltration of M1 macrophages in subcutaneous tumors but had no effect on the infiltration of M2 macrophages, which might be due to the limited samples (Figures 6C–6F). These results indicated that *TSC22D3* inhibits the polarization and infiltration of M1-type macrophages, ultimately promoting tumor progression.

TSC22D3 alleviates NF-κB and NLRP3 activation in tumor cells

To investigate the underlying mechanism that *TSC22D3* attenuated the polarization and infiltration of M1 macrophages, we further investigated whether *TSC22D3* regulates inflammatory-related signaling pathways. We detected NF-κB and NLRP3 pathway-related proteins in *TSC22D3*-knockdown tumor cells and found that inhibition of *TSC22D3* led to the activation of phosphorylated p65 (P-p65) and phosphorylated nuclear factor-kappa B inhibitor alpha (P-IKBα) (Figures 7A and 7B). NLRP3 pathway-associated proteins (NLRP3 and pro-IL-1β) were also increased in *TSC22D3*-knockdown tumor cells (Figures 7C–7F). To further investigate the role of NLRP3 in regulating macrophage polarization, we used cell-conditioned medium for secreted protein assays. Knockdown of *TSC22D3* resulted in the increase of IL-1β cytokines in the supernatant of tumor cells compared with their wild-type cells, while there was no significant IL-18 secretion (Figures 7G and 7H). Together, these results confirmed that knockdown of *TSC22D3* promotes the activation of NF-κB and NLRP3-associated inflammatory signaling pathways, leading to the increase of IL-1β secretion from tumor cells, which in turn affects the polarization and infiltration of macrophages and ultimately promotes the proliferation of tumor cells.

DISCUSSION

Despite the extensive research conducted on *TSC22D3* in tumor biology, its role and implication in AML had not been explored. Hence, this study focuses on the potential role of *TSC22D3* in the immunity and prognosis of AML patients. Through bioinformatics analysis of RNA sequencing (RNA-seq) data from UCSC XENA and GEO databases, *TSC22D3* was found to exhibit high expression levels, suggesting its potential as an immune-related biomarker for AML. Additionally, it has been discovered that increased levels of *TSC22D3* in individuals with AML are linked to unfavorable cytogenetics risk, shorter survival rates, and a bleak prognosis.

TSC22D3 is a leucine zipper protein that functions as a transcriptional regulator.[20] Structurally, The TSC22D3 protein contains three main components: the N-terminal domain of the transcription start site, the leucine zipper, and the proline-rich C-terminal domain.[9] *TSC22D3* expression is stimulated by glucocorticoids and IL-10 and is thought to be critical in the anti-inflammatory and immunosuppressive effects of CD80 and CD86.[21] Furthermore, *TSC22D3* is a vital factor in controlling the differentiation, apoptosis, and cell cycle of immune cells.[11] Prior research has indicated that *TSC22D3* has the potential to hinder the proliferation and maturation of cancerous cells by obstructing the functions of critical inflammatory signaling agents, including CCL5 (RANTES) and macrophage inflammatory protein-1 alpha (MIP-1α).[21] Macrophage-derived TSC22D3 also functions as a transcriptional co-inhibition for the pathogen-associated molecular patterns (PAMPs), Toll-like receptor 2, and NF-κB, thereby mediating the
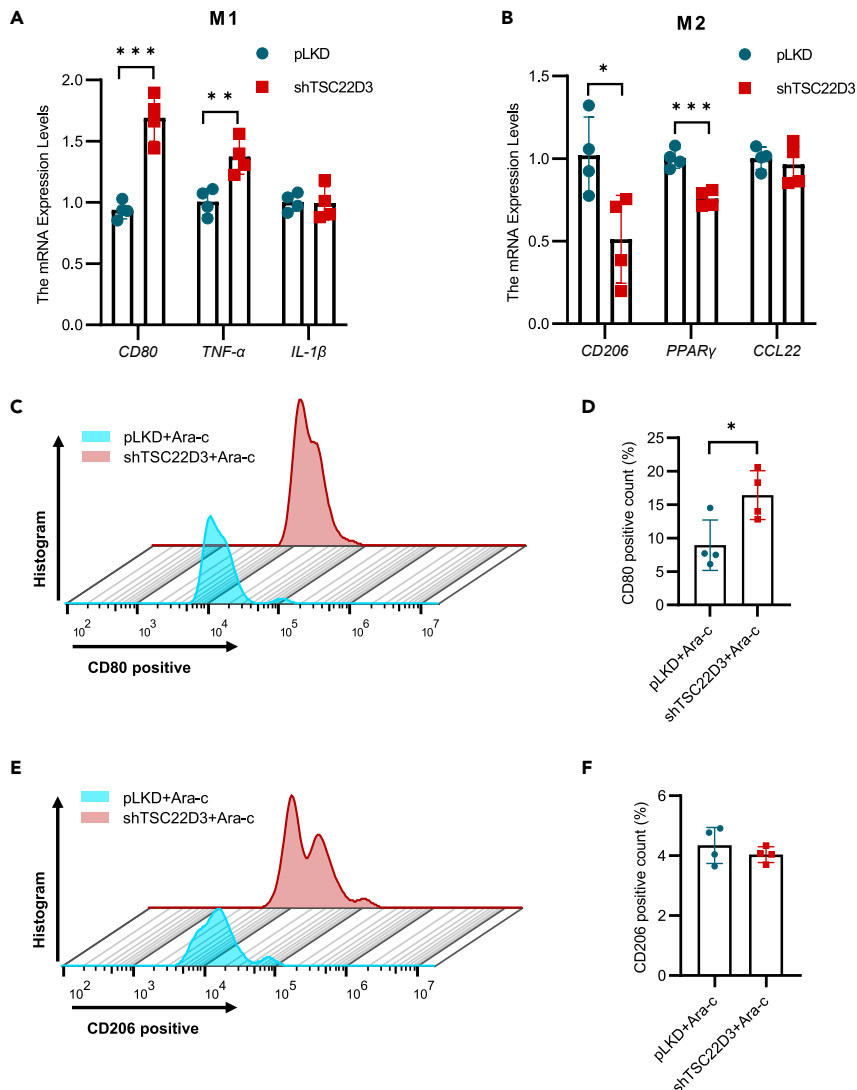
Figure 6. High expression of *TSC22D3* inhibits the polarization and infiltration of M1 macrophages

(A) RT-qPCR analysis of markers of M1-type macrophages after co-culture (n = 4).

(B) RT-qPCR analysis of markers of M2-type macrophages after co-culture (n = 4).

(C) The staggered offset histogram analysis showed M1 macrophages infiltration in the CDX model.

(D) Quantitative statistical analysis of M1 macrophages infiltration percentage (n = 4).

(E) The staggered offset histogram analysis showed M2 macrophages infiltration in the CDX model.

(F) Quantitative statistical analysis of M2 macrophages infiltration percentage (n = 4). Data were expressed as mean ± SD (A, B, D, and F). Student's t test (A, B, D, and F) for two groups comparison. Significant markers: *, p < 0.05; **, p < 0.01; ***, p < 0.001.

suppression of macrophage and anti-inflammatory effects.[21] Furthermore, L-GILZ, the protein isoform encoding TSC22D3, can promote the activation of p53 by competitively binding MDM2, thereby inhibiting tumor growth.[16] Conversely, another study has suggested that TSC22D3 may enhance the phosphorylation and activity of AKT in ovarian cancer cells, leading to increased tumor proliferation and metastasis.[12] Moreover, the increased expression of *TSC22D3* induced by glucocorticoids can attenuate anti-cancer immunity and promote tumor recurrence.[18] In present study, we observed a significant abundance of *TSC22D3* expression in AML patients (Figure 1), and high levels of *TSC22D3* are linked to unfavorable clinical outcomes (Figure 3), which was consistent with a recent bioinformatics study.[19] Given the limited knowledge available regarding the function of *TSC22D3*, we conducted functional annotation based on GO and GSEA analysis. Our results showed that TSC22D3 is involved in the regulation of
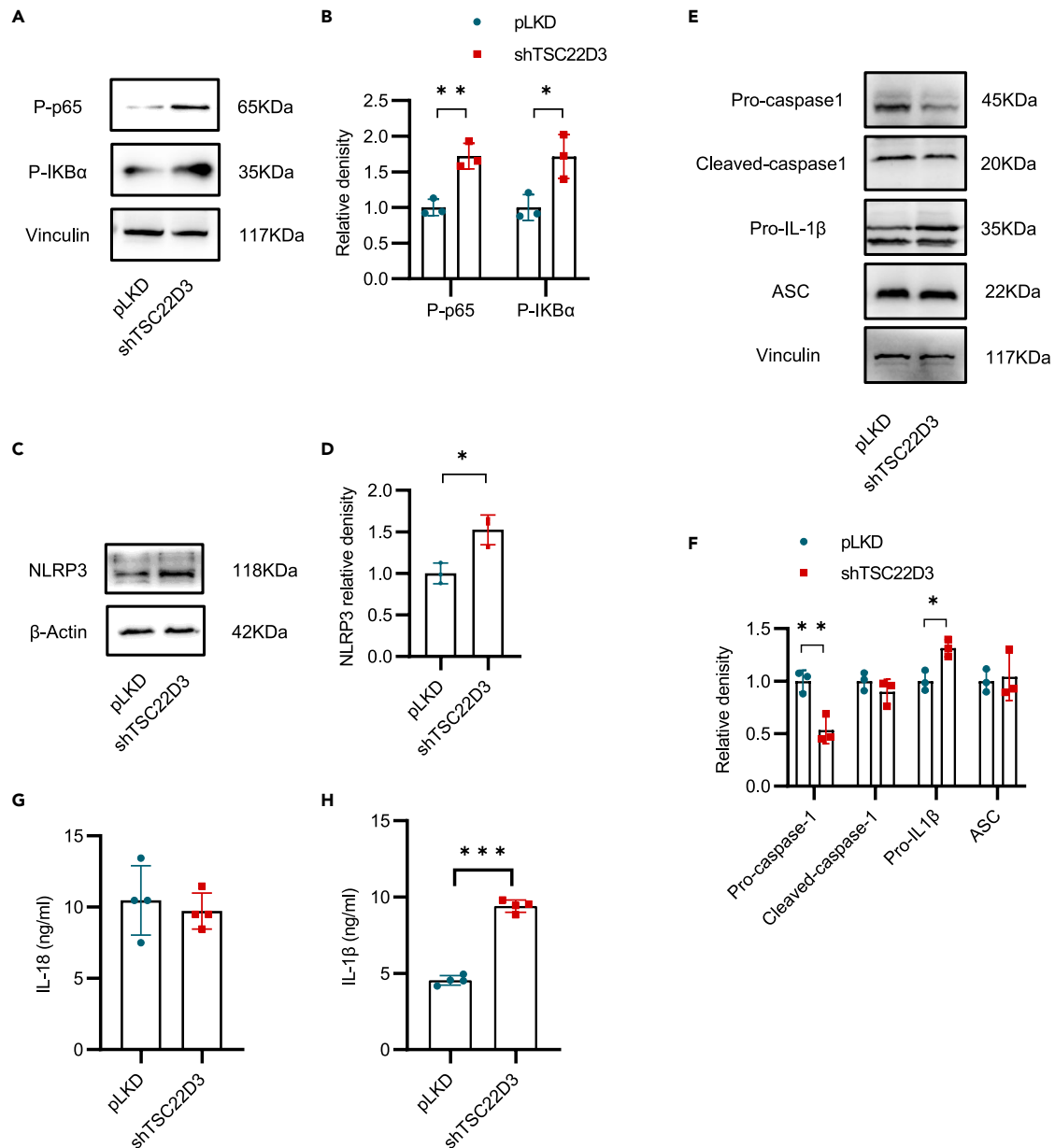
Figure 7. High expression of *TSC22D3* inhibits the activation of NF-κB and NLRP3 signaling pathways

(A) Western blot analysis of protein expression levels of P-p65 and P-IKBα in Hel cells after transfection.

(B) The normalized quantification of P-p65 and P-IKBα band density compared to vinculin (n = 3).

(C) Western blot analysis of protein expression levels of NLRP3 in Hel cells after transfection.

(D) The normalized quantification of NLRP3 band density compared to β-Actin (n = 3).

(E) Western blot analysis of protein expression levels of NLRP3 pathway-related molecular in Hel cells after transfection.

(F) The normalized quantification of NLRP3 pathway-related molecular band density compared to vinculin (n = 3).

(G and H) Elisa detected IL-1β and IL-18 concentrations in the supernatant of the transfected cell supernatant medium (n = 4). Data were expressed as mean ± SD (B, D, F, G, and H). Student's t test (B, D, F, G, and H) for two groups comparison. Significant markers: *, $p < 0.05$; **, $p < 0.01$; ***, $p < 0.001$.

inflammation and immunity (Figure 2), suggesting that *TSC22D3* may contribute to the advancement of AML by stimulating these signaling pathways.[22,23] Meanwhile, inhibition of TSC22D3 expression significantly impeded AML cell proliferation (Figure 4), affected the cell cycle via the p53 pathway, and increased cell sensitivity to Ara-c treatment (Figure 5). The prognostic significance of TSC22D3 in AML

was further suggested. *TSC22D3* is correlated with a negative prognosis for AML and contributes to the progression of the disease.

TSC22D3 encodes a protein that functions as important anti-inflammatory and immunosuppressive processes. Previous studies showed that immune cells can modify the carcinogenic properties of tumor cells and play crucial roles in the advancement of tumors.[24] Among those immune cells, macrophage is an important player in regulating AML tumor microenvironment.[25–27] It is noteworthy that tumor cells themselves can attract anti-inflammatory M2-type macrophages to promote the immune escape,[28] while the M1-type macrophages may help to suppress the development of AML disease.[29] In the present study, we found that *TSC22D3* positively correlated with macrophage infiltration (Figure 2B), and the knockdown of *TSC22D3* promoted polarization and infiltration of M1-type macrophage (Figure 6). These findings illustrated the close association between *TSC22D3* and immunoinfiltration in AML, potentially leading to immune evasion by changing the tumor microenvironment.

Previous studies showed that NF-κB is controversial in immune responses in tumor microenvironment,[30–33] which can either promote or inhibit the progression of tumors.[34,35] IL-1β, a downstream regulatory molecule of NF-κB, also has critical roles in tumor development,[36] by promoting the polarization of M1 macrophages.[37] This study revealed that *TSC22D3* led to the inhibition of NF-κB and NLRP3 signaling pathways, which suppressed IL-1β secretion by cancer cells (Figure 7), attenuating the inflammatory environment in the tumor microenvironment. As a result, M1 macrophage polarization and infiltration are inhibited and the balance between M1 and M2 macrophages is disrupted, ultimately promoting the progression of AML.

In summary, our study demonstrated that high expression of TSC22D3 is significantly associated with poor survival and immune infiltration in AML patients. TSC22D3 promotes tumorigenesis and progression in AML by suppressing the inflammatory response, which may trigger the immune escape of tumor cells. Together, TSC22D3 is an immune modulator of AML, which provides a new perspective to further investigate the pathogenesis of AML and tumor immune escape.

Limitations of the study

Although the present study revealed the role of *TSC22D3* in AML prognosis and immunoinfiltration, some limitations still require attention. Firstly, our study has not used the primary AML samples to validate our results; analysis of clinical patient specimens from newly diagnosed and relapsed patients is critical to better elucidate the role of *TSC22D3* in the disease process in the future. Secondly, we need to increase the quantity of cell lines to verify the functional role of *TSC22D3* in AML cells in multiple ways. Additionally, it would be beneficial to analyze RNA-seq in *TSC22D3*-knockdown cells to clarify possible downstream molecular mechanisms. Finally, to better elucidate the effect of *TSC22D3* on immunoinfiltration, humanized mouse models should be used to construct AML disease models.

STAR★METHODS

Detailed methods are provided in the online version of this paper and include the following:

- KEY RESOURCES TABLE
- RESOURCE AVAILABILITY
  - Lead contact
  - Materials availability
  - Data and code availability
- EXPERIMENTAL MODEL AND STUDY PARTICIPANT DETAILS
  - Human samples
  - Cell lines
  - Mouse models
- METHOD DETAILS
  - Data source, collation, and differential expression analysis
  - Gene Ontology (GO), immunoinfiltration, and gene set enrichment analysis (GSEA)
  - Establishment and prediction of a prognostic model
  - RT-qPCR
  - Western blotting

- ○ Short hairpin RNA (shRNA) knockdown
- ○ Lentiviral production and transduction
- ○ Cell viability assay
- ○ Annexin V and 7-AAD staining
- ○ Cell cycle analysis
- ○ THP1-induced differentiation macrophages
- ○ Co-culture
- ○ Preparation of single-cell suspension of mouse tumor tissue
- ○ Macrophages infiltration analysis
- ○ Enzyme-linked immunosorbent assay (Elisa)
- ● QUANTIFICATION AND STATISTICAL ANALYSIS

SUPPLEMENTAL INFORMATION

Supplemental information can be found online at https://doi.org/10.1016/j.isci.2023.107451.

AUTHOR CONTRIBUTIONS

Yang Li, Yang Liang, and Lingling Shu designed experiments; Yang Li, Hanying Huang, and Ziang Zhu performed experiments; Yang Li, Hanying Huang, Ziang Zhu, and Shuzhao Chen analyzed data; Yang Li and Lingling Shu edited the manuscript.

DECLARATION OF INTERESTS

The authors declare no conflict of interest.

INCLUSION AND DIVERSITY

We support inclusive, diverse, and equitable conduct of research.

REFERENCES

1. Miller, K.D., Fidler-Benaoudia, M., Keegan, T.H., Hipp, H.S., Jemal, A., and Siegel, R.L. (2020). Cancer statistics for adolescents and young adults, 2020. CA A Cancer J. Clin. *70*, 443–459. https://doi.org/10.3322/caac.21637.

2. Miller, K.D., Nogueira, L., Mariotto, A.B., Rowland, J.H., Yabroff, K.R., Alfano, C.M., Jemal, A., Kramer, J.L., and Siegel, R.L. (2019). Cancer treatment and survivorship statistics, 2019. CA A Cancer J. Clin. *69*, 363–385. https://doi.org/10.3322/caac.21565.

3. Walker, C.J., Kohlschmidt, J., Eisfeld, A.K., Mrózek, K., Liyanarachchi, S., Song, C., Nicolet, D., Blachly, J.S., Bill, M., Papaioannou, D., et al. (2019). Genetic Characterization and Prognostic Relevance of Acquired Uniparental Disomies in Cytogenetically Normal Acute Myeloid Leukemia. Clin. Cancer Res. *25*, 6524–6531. https://doi.org/10.1158/1078-0432.Ccr-19-0725.

4. Taylor, J., Xiao, W., and Abdel-Wahab, O. (2017). Diagnosis and classification of hematologic malignancies on the basis of genetics. Blood *130*, 410–423. https://doi.org/10.1182/blood-2017-02-734541.

5. D'Adamio, F., Zollo, O., Moraca, R., Ayroldi, E., Bruscoli, S., Bartoli, A., Cannarile, L., Migliorati, G., and Riccardi, C. (1997). A new dexamethasone-induced gene of the leucine zipper family protects T lymphocytes from TCR/CD3-activated cell death. Immunity *7*, 803–812. https://doi.org/10.1016/s1074-7613(00)80398-2.

6. Ayroldi, E., Migliorati, G., Bruscoli, S., Marchetti, C., Zollo, O., Cannarile, L., D'Adamio, F., and Riccardi, C. (2001). Modulation of T-cell activation by the glucocorticoid-induced leucine zipper factor via inhibition of nuclear factor kappaB. Blood *98*, 743–753. https://doi.org/10.1182/blood.v98.3.743.

7. Mittelstadt, P.R., and Ashwell, J.D. (2001). Inhibition of AP-1 by the glucocorticoid-inducible protein GILZ. J. Biol. Chem. *276*, 29603–29610. https://doi.org/10.1074/jbc.M101522200.

8. Ayroldi, E., Zollo, O., Macchiarulo, A., Di Marco, B., Marchetti, C., and Riccardi, C. (2002). Glucocorticoid-induced leucine zipper inhibits the Raf-extracellular signal-regulated kinase pathway by binding to Raf-1. Mol. Cell Biol. *22*, 7929–7941. https://doi.org/10.1128/mcb.22.22.7929-7941.2002.

9. Asselin-Labat, M.L., David, M., Biola-Vidamment, A., Lecoeuche, D., Zennaro, M.C., Bertoglio, J., and Pallardy, M. (2004). GILZ, a new target for the transcription factor FoxO3, protects T lymphocytes from

interleukin-2 withdrawal-induced apoptosis. Blood *104*, 215–223. https://doi.org/10.1182/blood-2003-12-4295.

10. Auphan, N., DiDonato, J.A., Rosette, C., Helmberg, A., and Karin, M. (1995). Immunosuppression by glucocorticoids: inhibition of NF-kappa B activity through induction of I kappa B synthesis. Science *270*, 286–290. https://doi.org/10.1126/science.270.5234.286.

11. Ronchetti, S., Migliorati, G., and Riccardi, C. (2015). GILZ as a Mediator of the Anti-Inflammatory Effects of Glucocorticoids. Front. Endocrinol. *6*, 170. https://doi.org/10.3389/fendo.2015.00170.

12. Redjimi, N., Gaudin, F., Touboul, C., Emilie, D., Pallardy, M., Biola-Vidamment, A., Fernandez, H., Prévot, S., Balabanian, K., and Machelon, V. (2009). Identification of glucocorticoid-induced leucine zipper as a key regulator of tumor cell proliferation in epithelial ovarian cancer. Mol. Cancer *8*, 83. https://doi.org/10.1186/1476-4598-8-83.

13. Joha, S., Nugues, A.L., Hétuin, D., Berthon, C., Dezitter, X., Dauphin, V., Mahon, F.X., Roche-Lestienne, C., Preudhomme, C., Quesnel, B., and Idziorek, T. (2012). GILZ inhibits the mTORC2/AKT pathway in BCR-ABL(+) cells. Oncogene *31*, 1419–1430. https://doi.org/10.1038/onc.2011.328.

14. Grugan, K.D., Ma, C., Singhal, S., Krett, N.L., and Rosen, S.T. (2008). Dual regulation of glucocorticoid-induced leucine zipper (GILZ) by the glucocorticoid receptor and the PI3-kinase/AKT pathways in multiple myeloma. J. Steroid Biochem. Mol. Biol. *110*, 244–254. https://doi.org/10.1016/j.jsbmb.2007.11.003.

15. Bruscoli, S., Donato, V., Velardi, E., Di Sante, M., Migliorati, G., Donato, R., and Riccardi, C. (2010). Glucocorticoid-induced leucine zipper (GILZ) and long GILZ inhibit myogenic differentiation and mediate anti-myogenic effects of glucocorticoids. J. Biol. Chem. *285*, 10385–10396. https://doi.org/10.1074/jbc.M109.070136.

16. Ayroldi, E., Petrillo, M.G., Bastianelli, A., Marchetti, M.C., Ronchetti, S., Nocentini, G., Ricciotti, L., Cannarile, L., and Riccardi, C. (2015). L-GILZ binds p53 and MDM2 and suppresses tumor growth through p53 activation in human cancer cells. Cell Death Differ. *22*, 118–130. https://doi.org/10.1038/cdd.2014.129.

17. Ayroldi, E., Petrillo, M.G., Marchetti, M.C., Cannarile, L., Ronchetti, S., Ricci, E., Cari, L., Avenia, N., Moretti, S., Puxeddu, E., and Riccardi, C. (2018). Long glucocorticoid-induced leucine zipper regulates human thyroid cancer cell proliferation. Cell Death Dis. *9*, 305. https://doi.org/10.1038/s41419-018-0346-y.

18. Yang, H., Xia, L., Chen, J., Zhang, S., Martin, V., Li, Q., Lin, S., Chen, J., Calmette, J., Lu, M., et al. (2019). Stress-glucocorticoid-TSC22D3 axis compromises therapy-induced antitumor immunity. Nat. Med. *25*, 1428–1441. https://doi.org/10.1038/s41591-019-0566-4.

19. Xu, X., Sun, R., Li, Y., Wang, J., Zhang, M., Xiong, X., Xie, D., Jin, X., and Zhao, M. (2023). Comprehensive bioinformatic analysis of the expression and prognostic significance of TSC22D domain family genes in adult acute myeloid leukemia. BMC Med. Genom. *16*, 117. https://doi.org/10.1186/s12920-023-01550-7.

20. Ayroldi, E., and Riccardi, C. (2009). Glucocorticoid-induced leucine zipper (GILZ): a new important mediator of glucocorticoid action. Faseb. J. *23*, 3649–3658. https://doi.org/10.1096/fj.09-134684.

21. Berrebi, D., Bruscoli, S., Cohen, N., Foussat, A., Migliorati, G., Bouchet-Delbos, L., Maillot, M.C., Portier, A., Couderc, J., Galanaud, P., et al. (2003). Synthesis of glucocorticoid-induced leucine zipper (GILZ) by macrophages: an anti-inflammatory and immunosuppressive mechanism shared by glucocorticoids and IL-10. Blood *101*, 729–738. https://doi.org/10.1182/blood-2002-02-0538.

22. Zhong, C., Wang, R., Hua, M., Zhang, C., Han, F., Xu, M., Yang, X., Li, G., Hu, X., Sun, T., et al. (2021). NLRP3 Inflammasome Promotes the Progression of Acute Myeloid Leukemia via IL-1β Pathway. Front. Immunol. *12*, 661939. https://doi.org/10.3389/fimmu.2021.661939.

23. Fisher, D.A.C., Fowles, J.S., Zhou, A., and Oh, S.T. (2021). Inflammatory Pathophysiology as a Contributor to Myeloproliferative Neoplasms. Front. Immunol. *12*, 683401. https://doi.org/10.3389/fimmu.2021.683401.

24. Güç, E., and Pollard, J.W. (2021). Redefining macrophage and neutrophil biology in the metastatic cascade. Immunity *54*, 885–902. https://doi.org/10.1016/j.immuni.2021.03.022.

25. Dalton, W.B., Ghiaur, G., and Resar, L.M. (2022). Taking the STING out of acute myeloid leukemia through macrophage-mediated phagocytosis. J. Clin. Invest. *132*, e157434. https://doi.org/10.1172/jci157434.

26. Li, W., Wang, F., Guo, R., Bian, Z., and Song, Y. (2022). Targeting macrophages in hematological malignancies: recent advances and future directions. J. Hematol. Oncol. *15*, 110. https://doi.org/10.1186/s13045-022-01328-x.

27. Weiskopf, K., and Weissman, I.L. (2015). Macrophages are critical effectors of antibody therapies for cancer. mAbs *7*, 303–310. https://doi.org/10.1080/19420862.2015.1011450.

28. Guo, X., Zhao, Y., Yan, H., Yang, Y., Shen, S., Dai, X., Ji, X., Ji, F., Gong, X.G., Li, L., et al. (2017). Single tumor-initiating cells evade immune clearance by recruiting type II macrophages. Genes Dev. *31*, 247–259. https://doi.org/10.1101/gad.294348.116.

29. Yang, X., Feng, W., Wang, R., Yang, F., Wang, L., Chen, S., Ru, Y., Cheng, T., and Zheng, G. (2018). Repolarizing heterogeneous leukemia-associated macrophages with more M1 characteristics eliminates their pro-leukemic effects. OncoImmunology *7*, e1412910. https://doi.org/10.1080/2162402x.2017.1412910.

30. Pflug, K.M., and Sitcheran, R. (2020). Targeting NF-κB-Inducing Kinase (NIK) in Immunity, Inflammation, and Cancer. Int. J. Mol. Sci. *21*, 8470. https://doi.org/10.3390/ijms21228470.

31. Greten, F.R., and Grivennikov, S.I. (2019). Inflammation and Cancer: Triggers, Mechanisms, and Consequences. Immunity *51*, 27–41. https://doi.org/10.1016/j.immuni.2019.06.025.

32. Atretkhany, K.S.N., Drutskaya, M.S., Nedospasov, S.A., Grivennikov, S.I., and Kuprash, D.V. (2016). Chemokines, cytokines and exosomes help tumors to shape inflammatory microenvironment. Pharmacol. Ther. *168*, 98–112. https://doi.org/10.1016/j.pharmthera.2016.09.011.

33. Quail, D.F., and Joyce, J.A. (2013). Microenvironmental regulation of tumor progression and metastasis. Nat. Med. *19*, 1423–1437. https://doi.org/10.1038/nm.3394.

34. Perkins, N.D. (2004). NF-kappaB: tumor promoter or suppressor? Trends Cell Biol. *14*, 64–69. https://doi.org/10.1016/j.tcb.2003.12.004.

35. Chen, F., Beezhold, K., and Castranova, V. (2008). Tumor promoting or tumor suppressing of NF-kappa B, a matter of cell context dependency. Int. Rev. Immunol. *27*, 183–204. https://doi.org/10.1080/08830180802130327.

36. Bent, R., Moll, L., Grabbe, S., and Bros, M. (2018). Interleukin-1 Beta-A Friend or Foe in Malignancies? Int. J. Mol. Sci. *19*, 2155. https://doi.org/10.3390/ijms19082155.

37. Wu, J., Li, K., Peng, W., Li, H., Li, Q., Wang, X., Peng, Y., Tang, X., and Fu, X. (2019). Autoinducer-2 of Fusobacterium nucleatum promotes macrophage M1 polarization via TNFSF9/IL-1β signaling. Int. Immunopharm. *74*, 105724. https://doi.org/10.1016/j.intimp.2019.105724.

38. Wickham, H. (2016). ggplot2 : Elegant Graphics for Data Analysis, 2016 Edition (Springer-Verlag).

39. Love, M.I., Huber, W., and Anders, S. (2014). Moderated estimation of fold change and dispersion for RNA-seq data with DESeq2. Genome Biol. *15*, 550. https://doi.org/10.1186/s13059-014-0550-8.

40. Yu, G., Wang, L.G., Han, Y., and He, Q.Y. (2012). clusterProfiler: an R package for comparing biological themes among gene clusters. OMICS *16*, 284–287. https://doi.org/10.1089/omi.2011.0118.

41. Hänzelmann, S., Castelo, R., and Guinney, J. (2013). GSVA: gene set variation analysis for microarray and RNA-seq data. BMC Bioinf. *14*, 7. https://doi.org/10.1186/1471-2105-14-7.

42. Blanche, P., Dartigues, J.F., and Jacqmin-Gadda, H. (2013). Estimating and comparing time-dependent areas under receiver operating characteristic curves for censored event times with competing risks. Stat. Med. *32*, 5381–5397. https://doi.org/10.1002/sim.5958.

43. Vivian, J., Rao, A.A., Nothaft, F.A., Ketchum, C., Armstrong, J., Novak, A., Pfeil, J., Narkizian, J., Deran, A.D., Musselman-Brown, A., et al. (2017). Toil enables reproducible, open source, big biomedical data analyses. Nat. Biotechnol. *35*, 314–316. https://doi.org/10.1038/nbt.3772.

44. Bindea, G., Mlecnik, B., Tosolini, M., Kirilovsky, A., Waldner, M., Obenauf, A.C., Angell, H., Fredriksen, T., Lafontaine, L., Berger, A., et al. (2013). Spatiotemporal dynamics of intratumoral immune cells reveal the immune landscape in human cancer. Immunity *39*, 782–795. https://doi.org/10.1016/j.immuni.2013.10.003.

STAR★METHODS

KEY RESOURCES TABLE

REAGENT or RESOURCE	SOURCE	IDENTIFIER
Antibodies		
Rabbit Polyclonal anti-TSC22D3	Signalway Antibody	Cat#39175
Rabbit Monoclonal anti-β-Actin	Signalway Antibody	Cat#52901
Goat Polyclonal anti-Rabbit IgG (H&L) HRP	Signalway Antibody	Cat#L35009
Rabbit Monoclonal anti-PCNA (D3H8P) XP®	Cell Signaling Technology	Cat#13110; RRID:AB_2636979
Rabbit Monoclonal anti- Phospho-NF-kappaB p65 (Ser536) (93H1)	Cell Signaling Technology	Cat#3033; RRID:AB_331284
Rabbit Monoclonal anti-IKB alpha (phospho S36)	Abcam	Cat#ab133462; RRID:AB_2801653
Rabbit Monoclonal anti-NLRP3	Abcam	Cat#ab263899; RRID:AB_2889890
Rabbit Monoclonal anti-pro Caspase-1 + p10 + p12	Abcam	Cat#ab179515; RRID:AB_2884954
Rabbit Monoclonal anti-p53	PTM Biolabs	Cat#PTM-6319
Rabbit Polyclonal anti-Caspase-1/Cleaved Caspase-1	Wanleibio	Cat#WL03450
Rabbit Polyclonal anti-pro IL-1β	Wanleibio	Cat#WL02257; RRID:AB_2894987
Rabbit Polyclonal anti-TMS1/ASC	Wanleibio	Cat#02462; RRID:AB_2935861
Rabbit Polyclonal anti-Vinculin	Wanleibio	Cat#03922
Monoclonal Pacific Blue™ anti-mouse/human CD11b	BioLegend	Cat#101224; RRID:AB_755986
Monoclonal FITC anti-mouse F4/80 antibody	BioLegend	Cat#123107; RRID:AB_893500
Monoclonal PE anti-mouse CD80 antibody	BioLegend	Cat#104707; RRID:AB_313128
Monoclonal APC anti-mouse CD206 (MMR) antibody	BioLegend	Cat#141707; RRID:AB_10896057
Bacterial and virus strains		
Stbl3 competent cells	TSINGKE	Cat#TSC-C06
Chemicals, peptides, and recombinant proteins		
TRIzol® reagent	ThermoFisher	Cat#15596018
Universal antibody diluent	EpiZyme	Cat#PS119L
Annealing buffer	Beyotime	Cat#D0251
Ampicillin	MDbio	Cat#A010
Opti-MEM	ThermoFisher	Cat#31985070
CCK-8	Apex Bio	Cat#K1018
Cytarabine (Ara-c)	Apex BIO	Cat#A8405
Phorbol-12-myristate-13-acetate (PMA)	MCE	Cat#HY-18739
Recombinant human IFN-γ protein	NovoProtein	Cat#C014
Lipopolysaccharide (LPS)	Bioss	Cat#bs-8000P
Recombinant human IL-4 protein	NovoProtein	Cat#C050
Recombinant human IL-13 protein	NovoProtein	Cat#CC89
Matrigel	CELLada	Cat#CELLada-OM-2
Type I collagenase	Sigma	Cat#C0130
DNase I	Acmec	Cat#D61780
Red blood cell lysate	Beyotime	Cat#C3702
7-AAD Viability Staining Solution	BioLegend	Cat#420404
Critical commercial assays		
Fast Reverse Transcription kit	ESscience	Cat#RT001
2 x Super SYBR Green qPCR Master Mix (with ROX)	ESscience	Cat#QP002

Continued

REAGENT or RESOURCE	SOURCE	IDENTIFIER
Bicinchoninic acid (BCA) Protein Assay Kit	CWBIO	Cat#CW0014S
12.5% SDS-PAGE Gel Fast Preparation Kit	EpiZyme	Cat#PG113
*Age*I-HF	NEB	Cat#R3552L
*Eco*RI-HF	NEB	Cat#R3101V
T4 DNA ligase	NEB	Cat#M0201S
Endotoxin-Free Plasmid Extractor Kit	TIANGEN	Cat#DP118-02
lipofectamine 3000	Invitrogen	Cat#L3000015
7-AAD-APC-Annexin V Apoptosis Assay	Tonbo	Cat#20-6410-KIT
Cell Cycle Analysis kit	4Abio	Cat#FXP0211
Human IL-18 Elisa Kit	MultiSciences	Cat#EK118
Human IL-1β ELISA Kit	MultiSciences	Cat#EK101B
Deposited data		
TCGA and GTEx databases RNA sequencing data	UCSC XENA	https://xenabrowser.net/datapages/
GSE15061 and GSE13159 datasets sequencing data	GEO	http://www.ncbi.nlm.nih.gov/geo/
Original data and statistical description	This study	https://data.mendeley.com/datasets/tnbptc8yff/2
Experimental models: Cell lines		
Human: KG-1	Laboratory of Yang Liang	RRID:CVCL_0374
Human: MV-4-11	Laboratory of Yang Liang	RRID:CVCL_0064
Human: OCI-AML3	Laboratory of Yang Liang	RRID:CVCL_1844
Human: U937	Laboratory of Yang Liang	RRID:CVCL_0007
Human: Hel	Laboratory of Yuanbin Song	RRID:CVCL_0001
Human: THP1	Laboratory of Yuanbin Song	RRID:CVCL_0006
Human: 293T	Laboratory of Yang Liang	RRID:CVCL_0063
Experimental models: Organisms/strains		
Mouse: BALB/c nude	Sun Yat-sen University Cancer Center	N/A
Oligonucleotides		
RT-qPCR primers see Table S1	This study	N/A
shRNA sequences see Table S2	This study	N/A
Recombinant DNA		
pLKD-U6-MCS-CMV-EGFP-2A-Puro	Umine-bio	Cat#G0202296-1
pLKD-U6-shRNA (non-targeting)-CMV-EGFP-2A-Puro	This study	N/A
pLKD-U6-shRNA (*TSC22D3*)-CMV-EGFP-2A-Puro	This study	N/A
psPAX2	Laboratory of Yang Liang	N/A
pVSVG	Laboratory of Yang Liang	N/A
Software and algorithms		
ggplot2 (v3.3.3)	Wickham[38]	https://cran.r-project.org/web/packages/ggplot2/index.html
DESeq2 (v1.26.0)	Love et al.[39]	https://bioconductor.org/packages/release/bioc/html/DESeq2.html
clusterProfiler (v3.14.3)	Yu et al.[40]	http://bioconductor.org/packages/release/bioc/html/clusterProfiler.html
GSVA (v1.34.0)	Hänzelmann et al.[41]	https://www.bioconductor.org/packages/release/bioc/html/GSVA.html

Continued

REAGENT or RESOURCE	SOURCE	IDENTIFIER
timeROC (v0.4)	Blanche et al.[42]	https://cran.r-project.org/web/packages/timeROC/index.html
RStudio (v3.6.3)	Posit Software Inc., USA	https://posit.co/download/rstudio-desktop/
ImageJ (v1.8.0)	National Institutes of Health, USA	https://downloads.imagej.net/fiji/latest/fiji-win64.zip
FlowJo (v10.8.1)	BD Biosciences	https://www.flowjo.com/solutions/flowjo/downloads
GraphPad Prism 9.5	GraphPad Software Inc., CA, USA	https://www.graphpad.com/

RESOURCE AVAILABILITY

Lead contact

Further information and requests for resources and reagents should be directed to and will be fulfilled by the lead contact, Lingling Shu (shull@sysucc.org.cn).

Materials availability

This study did not generate new unique reagents.

Data and code availability

- This paper analyzes existing, publicly available data. These accession numbers for the datasets are listed in the key resources table.

- All codes used for the bioinformatics analysis in this study were derived from existing software and algorithms, as listed in the key resources table. This paper does not report original code.

- Original data and statistical description have been saved as the Mendeley dataset (https://doi.org/10.17632/tnbptc8yff.2). The link is listed in the key resources table. Any additional information required to reanalyze the data reported in this paper is available from the lead contact upon request.

EXPERIMENTAL MODEL AND STUDY PARTICIPANT DETAILS

Human samples

All RNA-seq data and clinical characteristics of human samples in this study were obtained from UCSC XENA (https://xenabrowser.net/datapages/) and Gene Expression Omnibus (GEO) (http://www.ncbi.nlm.nih.gov/geo/) public databases.

Cell lines

KG-1, MV-4-11, OCI-AML3, U937, and 293T cell lines were generously gifted by Professor Yang Liang (State Key Laboratory of South China, Sun Yat-sen University cancer center). Hel and THP1 cell lines were obtained from Professor Yuanbin Song (State Key Laboratory of South China, Sun Yat-sen University cancer center). Details of the cell lines are shown in Table S5. KG-1, MV-4-11, OCI-AML3, U937, Hel, and THP1 cell lines were grown in RPMI medium (Gibco, Cat#C11875500BT). The 293T cell line was cultured using DMEM medium (Gibco, Cat#C11995500BT) and passaged with 0.25% Trypsin-EDTA (Gibco, Cat#25200072). All cell lines were cultured under controlled conditions at 37°C in 5% CO_2 and complemented with 10% Fetal bovine serum (FBS) (WISENT, Cat#086-150), as well as 1% penicillin (with a final concentration of 100 U/ml) and 1% streptomycin (with a final concentration of 100 μg/ml) (Gibco, Cat#15140122). All cell lines were identified by short tandem repeat and tested negative for mycoplasma.

Mouse models

The control and *TSC22D3* knockdown groups were mixed with an equal volume of Matrigel (CELLada, Cat#CELLada-OM-2) and implanted by subcutaneous injection into the right dorsum of 4–6-week-old male BALB/c nude mice (5 × 10^6 cells/mouse, 150 ul) (Mice were provided by Sun Yat-sen University Cancer Center) to establish a cell-derived xenograft model (CDX). When the tumor reached a measurable size, mice were treated with intraperitoneal injection of 20 mg/kg Ara-c every three days. The tumor dimensions

including the longest diameter (D), shortest diameter (D), as well as its height (H), were measured every five days using vernier calipers. The formula (D*d*H) * $\pi/6$ was used to calculate the tumor volume. Mice were euthanized if they lost more than 20% of their body weight or if the tumor size exceeded 2 cm^3. The ethics of animal experiments in this study strictly followed the relevant provisions of the Guide for the Care and Use of Laboratory Animals published by the National Academic Press and was also approved by the Laboratory Animal Ethics Committee of Sun Yat-sen University Cancer Control Center (Approval number: L025504202209001).

METHOD DETAILS

Data source, collation, and differential expression analysis

RNA-seq data from TCGA and GTEx databases were downloaded from UCSC XENA database and converted to transcripts per million reads (TPM) format by Toil process uniformly.[43] The GSE15061 and GSE13159 datasets were obtained from GEO database. All data were converted to log2, and duplicate samples and samples with missing gene expression data were removed. The ggplot2 (v3.3.3) package was used for data visualization.[38] Based on the TCGA datasets, DESeq2 (v1.26.0) package was used to detect DEGs between patients with high versus low *TSC22D3*.[39] Genes that met the criteria of having an adjusted |log2(FC)| > 1 and p.adj < 0.05 were considered statistically relevant.

Gene Ontology (GO), immunoinfiltration, and gene set enrichment analysis (GSEA)

The org.Hs.eg.db (v3.10.0) package and clusterProfiler (v3.14.3) package were used to perform GO analysis.[40] Immunoinfiltration analysis of *TSC22D3* was performed by single sample GSEA (ssGSEA) with the GSVA (v1.34.0) package.[41] Inferring the relationship between *TSC22D3* and infiltration of 24 immune cells in the tumor microenvironment using Spearman correlation analysis.[44] Additionally, GSEA and visualization of DEGs with clusterProfiler (v3.14.3) package.[40] The condition that the False Discovery Rate (FDR) < 0.25 and p.adj < 0.05 was considered statistically significant enrichment by repeating the calculation 1000 times.

Establishment and prediction of a prognostic model

Kaplan-Meier (K-M) curves analysis of 8-year Overall survival (OS) differences between high versus low *TSC22D3* expression groups and various mutation genotype subgroups (Subgroups with a total sample number of less than 5 were not included in the analysis). Clinical characteristics with p-values less than 0.1 in univariate Cox regression analysis were considered for multivariate Cox regression analysis. All statistical p-values less than 0.05 were considered significant. The timeROC (v0.4) package[42] and ggplot2 (v3.3.3) package[38] were used to conduct the ROC model. Calibration plots and nomograms were constructed with the RMS (v6.2-0) and survivor (v3.2-10) packages.

RT-qPCR

The cell samples underwent two washes with phosphate-buffered solution (PBS) (MCE, Cat#C10010500BT) at 1000 rpm for 5 minutes. Total RNA was extracted from cells according to the standard protocol using TRIzol® reagent (ThermoFisher, Cat#15596018). RNase-free water was utilized to dissolve RNA, and the RNA quality and concentration were determined with the NanoDrop microspectrophotometer (ThermoFisher, Cat#840-317500). Reverse transcription of 1ug total RNA to cDNA using the Fast Reverse Transcription kit (ESscience, Cat#RT001) according to the standard protocol. The 2 x Super SYBR Green qPCR Master Mix (with ROX) (ESscience, Cat#QP002) and Bio-Rad Quantitative real-time PCR instrument (Bio-Rad, Cat#CFX96 Touch) were used for conducting quantitative real-time PCR. The appropriate annealing temperature was set according to the primer temperature. The primer sequences used to identify gene expression in human *GAPDH*, *TSC22D3*, *CD68*, *CD80*, tumor necrosis factor-α (*TNF-α*), interleukin-1β (*IL-1β*), *CD206*, *PPARγ*, and *CCL22* are detailed in Table S1. Statistical analysis of the results was performed using the 2^-$\Delta\Delta$Ct method.

Western blotting

The cells underwent two washes with PBS and were subsequently lysed on ice for 40 minutes in RIPA buffer, which contained 1% phenyl methane sulfonyl fluoride (PMSF) (UBIO, Cat#UW0103) and 1% Phosphatase Inhibitor Cocktail (CWBIO, Cat#CW2383S). The protein concentration was measured using the bicinchoninic acid (BCA) Protein Assay Kit (CWBIO, Cat#CW0014S) following the standard protocol and detected with a microplate reader at a wavelength of 562 nm. Adding 5 × loading buffer (Fudebio, Cat#FD006) to the protein samples and heat at 95°C for 15 minutes in a metal bath. Using the 12.5% SDS-PAGE Gel Fast

Preparation Kit (EpiZyme, Cat#PG113) to separate protein samples, pre-marker proteins (ThermoFisher, Cat#26616) were used to mark protein locations. Polyvinylidene fluoride (PVDF) membranes with 0.22 μm (for molecular weights less than 20 KDa) (Biosharp, Cat#BS-PVDF-22) or 0.45 μm (for molecular weights greater than 20 KDa) (Merck Millipore, Cat#IPVH00010) pore size was activated by 100% methanol (Macklin, Cat#M813895) for 5 minutes. The isolated proteins were then transferred from the gel to the PVDF membrane using the BIO-RAD wet transfer system and immobilized. The PVDF membranes were blocked using 5% skim milk (Wako, Cat#190-12865) dissolved in TBST (20 mM Tris base (Sigma, Cat#V900483), 150 mM NaCl (Biofroxx, Cat#1249GR500), 0.1% Tween 20 (Solarbio, Cat#T8220), and pH = 7.6) buffer for 90 minutes at 25°C. Primary antibodies were incubated at 4°C overnight, while secondary antibodies were incubated at 25°C for 2 hours. Detailed dilution ratios of all antibodies see Table S6. Universal antibody diluent (EpiZyme, Cat#PS119L) was used to dilute all western blotting antibodies. The BIO-RAD chemiluminescence imaging system was used to detect protein expression, and ImageJ (National Institutes of Health, USA, v1.8.0) was used to analyze protein relative grayscale values.

Short hairpin RNA (shRNA) knockdown

The pLKD-U6-MCS-CMV-EGFP-2A-Puro (Umine-bio, Cat#G0202296-1) plasmid was used to construct the non-targeting shRNA vector (Designated as pLKD) and the targeting human *TSC22D3* shRNA vector (Designated as shTSC22D3). The targeting sequences are shown in Table S2. The empty plasmid was digested with *AgeI*-HF (NEB, Cat#R3552L) and *EcoRI*-HF (NEB, Cat#R3101V) restriction enzymes according to the standard protocol to create sticky ends and formed linear plasmids. The single-stranded cDNA was formed double-stranded DNA with sticky ends according to the standard protocol under annealing buffer (Beyotime, Cat#D0251). Double-stranded oligo and linear plasmids formed pLKD-U6-shRNA (non-targeting)-CMV-EGFP-2A-Puro and pLKD-U6-shRNA (*TSC22D3*)-CMV-EGFP-2A-Puro recombinant plasmids under the action of T4 DNA ligase (NEB, Cat#M0201S) according to the standard protocol. Stbl3 competent cells (TSINGKE, Cat#TSC-C06) were used to amplify the plasmids. The positive monoclonal screening was then performed on Luria-Bertani (LB) solid medium (containing 10 mg/ml Tryptone (Oxoid, Cat#LP0042B), 5 mg/ml Yeast extract power (Oxoid, Cat#LP0021B), 5 mg/ml NaCl, and 100 ug/ml Ampicillin (Amp) (MDbio, Cat#A010)) following the standard protocol. The Endotoxin-Free Plasmid Extractor Kit (TIANGEN, Cat#DP118-02) was used to extract and purify positive plasmids following the standard protocol. The plasmid's quality and concentration were determined with the NanoDrop microspectrophotometer (ThermoFisher, Cat#840-317500).

Lentiviral production and transduction

293T cells were cultured to produce viral fluid in Opti-MEM (ThermoFisher, Cat#31985070) containing DNA (Recombinant plasmids: psPAX2: pVSVG = 3: 2: 1) and lipofectamine 3000 (Invitrogen, Cat#L3000015) for 8 hours following the standard protocol. After replacing the complete medium, the cells were incubated for an additional 36, 48, and 72 hours. The conditioning medium was filtered through a 0.45 μm filter and infected with Hel cells for 24 hours. EGFP-positive cells were observed and sorted using a fluorescence microscope and the Beckman Moflo Astrios EQ system after 4 days of infection.

Cell viability assay

EC50, proliferation, and viability were detected using the CCK-8 (Apex Bio, Cat#K1018) method. The control and *TSC22D3* knockdown groups cells were cultured in 96-well plates (Corning, Cat#3599) at a density of 1 x 10^4 cells/well for cell proliferation and at a density of 5 x 10^4 cells/well for cell viability and EC50 assays. The cells were treated with 100 nM Cytarabine (Ara-c) (Apex BIO, Cat#A8405) for 4 days, with or without treatment. EC50 was determined using isometrically diluted concentrations of Ara-c for 48 hours. Optical density (OD) was then measured using a Biotech-Epoch microplate reader with a wavelength of 450 nm.

Annexin V and 7-AAD staining

6-well plates (Corning, Cat#3516) were seeded with cells from the control and *TSC22D3* knockdown groups with a density of 1 × 10^6 cells in each well. Cells were harvested and washed three times with ice-cold PBS for 5 minutes at 1000 rpm after 2 days of treatment with 100 nM Ara-c. Apoptotic rates were analyzed using the 7-AAD-APC-Annexin V Apoptosis Assay (Tonbo, Cat#20-6410-KIT) according to standard protocols and the Beckman Cytoflex lx system. Results were analyzed using FlowJo (BD Biosciences, v10.8.1) software.

Cell cycle analysis

The control and *TSC22D3* knockdown group cells were cultured in Opti-MEM medium for 24 hours to synchronize the cell cycles. The medium was subsequently altered, and cells were incubated for 48 hours with or without 100 nM Ara-c. The cell cycle was analyzed with the Cell Cycle Analysis kit (4Abio, Cat#FXP0211) and the Beckman Cytoflex lx system following the standard protocol. The results were analyzed using FlowJo (BD Biosciences, v10.8.1) software, and cell cycle model constraints were G2 peak = 2 G1, G1 coefficient of variation (CV) = G2 CV = 8.00.

THP1-induced differentiation macrophages

THP1 cells were seeded in 6-well plates at a density of 1 x 10^6 cells/well and treated with 185ng/ml phorbol-12-myristate-13-acetate (PMA) (MCE, Cat#HY-18739) for 6 hours to induce differentiation into M0 macrophages. To induce differentiation of cells into M1 macrophages, interferon-γ (IFN-γ) (NovoProtein, Cat#C014) at a concentration of 20 ng/ml and lipopolysaccharide (LPS) (Bioss, Cat#bs-8000P) at a concentration of 100 ng/ml were added. This was followed by incubation for 48 hours in the presence of PMA. Similarly, the cells were differentiated into M2 macrophages with 20 ng/ml interleukin-4 (IL-4) (NovoProtein, Cat#C050) and 20 ng/ml interleukin–13 (IL-13) (NovoProtein, Cat#CC89) stimulation for 48 hours. RT-qPCR to assess the expression levels of mRNA markers for M1 and M2 macrophages.

Co-culture

The direct co-culture system was used to evaluate the impact of *TSC22D3*-knocked tumor cells on macrophage polarization. THP1 cells were seeded in 6-well plates at a density of 1 x 10^6 cells/well. The cells were then differentiated into M0 macrophages through PMA stimulation for a period of 6 hours. *TSC22D3* knockdown Hel cells and their relative control were cultured with macrophages at a 1: 1 ratio with M1 polarizing stimulators (IFN-γ and LPS) or M2 polarizing stimulators (IL-4 and IL-13) for 48 hours in the continued presence of PMA. The Hel cell suspension and medium were then removed, and macrophages were washed three times with PBS before RNA extraction. RT-qPCR analysis was adopted to analyze the mRNA abundance of M1-or M2 macrophage-related genes.

Preparation of single-cell suspension of mouse tumor tissue

Tumor tissue was minced into small pieces of 1-3 mm^3 and then incubated in the complete medium that contained type I collagenase (final concentration 1 mg/ml) (Sigma, Cat#C0130) and DNase I (final concentration 100 U/ml) (Acmec, Cat#D61780) at 37°C with constant shaking (100 rpm) for 4 hours. The tissue suspension was washed three times with PBS at 1000 rpm for 5 minutes each after passing through a 70 μm cell strainer. Cells were lysed using a red blood cell lysate (Beyotime, Cat#C3702) and cells were allowed to stand on ice for 5 minutes. The single-cell suspension was obtained after three washes using PBS at 1000 rpm for 5 minutes.

Macrophages infiltration analysis

The samples underwent three rounds of washing with ice-cold PBS for 5 minutes at 1000 rpm. Flow cytometry staining buffer (PBS with 3% FBS) containing different flow cytometry antibodies was added. The 7-AAD Viability Staining Solution (BioLegend, Cat#420404, used 1: 100) was used to distinguish between living and dead cells. Myeloid cells were identified using CD11b antibody, while macrophages were labeled using F4/80 antibody. M1-type macrophages were marked with CD80 antibody, and M2-type macrophages were labeled with CD206 antibody. Detailed dilution ratios of all antibodies see Table S6. Macrophage infiltration in mouse subcutaneous tumor tissues was analyzed using the Beckman Cytoflex lx and FlowJo (BD Biosciences, v10.8.1) software.

Enzyme-linked immunosorbent assay (Elisa)

The control and *TSC22D3* knockdown group cells were plated at 5 × 10^5 cells per well in 6-well culture plates. After 4 days of culture, the supernatant was collected via 5-minute centrifugation at 1000 rpm. The Human IL-18 ELISA Kit (MultiSciences, Cat#EK118) and Human IL-1β ELISA Kit (MultiSciences, Cat#EK101B) were used to detect the cytokine levels in the media supernatant according to the standard protocol. Absorbance at 450 nm and 630 nm was measured using a Biotech-Epoch microplate reader. Statistics were analyzed using calibrated OD values, acquired by deducting the OD value at 630 nm from the OD value at 450 nm.

QUANTIFICATION AND STATISTICAL ANALYSIS

Shapiro-Wilk test was conducted to assess the normality of the data. Additionally, the homogeneity of variance was evaluated using Levene's test. Differences between the two groups were compared using Student's t-test or Wilcoxon rank sum test. The overall comparison of multiple groups was analyzed using one-way ANOVA test or Kruskal-Wallis's test. Meanwhile, the two-way repeated measures ANOVA was employed for two-factor group analysis. Bioinformatics analysis was performed using RStudio (Posit Software Inc., USA, v3.6.3) software for statistical analysis. All experimental data were statistically analyzed and plotted using GraphPad Prism 9.5 (GraphPad Software Inc., CA, USA) software. All experiments were repeated independently at least three times (n $\geq$ 3).